Hyaluronan Regulates Eyelid and Meibomian Gland Morphogenesis

Mingxia Sun,[1] Sudan Puri,[1] Geraint J. Parfitt,[2,3] Nadine Mutoji,[1] and Vivien J. Coulson-Thomas[1]

[1]College of Optometry, University of Houston, Houston, Texas, United States
[2]European Cancer Stem Cell Research Institute, Cardiff University, Cardiff, Wales, United Kingdom
[3]School of Optometry and Vision Sciences, Cardiff University, Wales, United Kingdom

Correspondence: Vivien J. Coulson-Thomas, College of Optometry, University of Houston, 4901 Calhoun Road, Houston, TX 77204-2020, USA;
vcoulsonthomas@gmail.com.

Submitted: March 8, 2018
Accepted: May 30, 2018

Citation: Sun M, Puri S, Parfitt GJ, Mutoji N, Coulson-Thomas VJ. Hyaluronan regulates eyelid and Meibomian gland morphogenesis. *Invest Ophthalmol Vis Sci*. 2018;59:3713–3727. https://doi.org/10.1167/iovs.18-24292

Purpose. The Meibomian gland (MG) produces the lipid layer of the tear film, and changes to the MG that lead to a decrease or alteration in lipid quality/content may lead to MG dysfunction, a major cause of evaporative dry eye disease with prevalence ranging from 39% to 50%. Little is known about the developmental cues that regulate MG morphogenesis and homeostasis. Our study investigates the role of hyaluronan (HA), a major extracellular matrix component, in eyelid formation and MG development and function.

Methods. Hyaluronan synthase (*Has*) knockout mice were used to determine the role of HA in the eyelid and MG. Eyelids were obtained during different developmental stages and MG morphology was analyzed. Tet-off H2B-GFP/K5tTA mice and 5-ethynyl-2′-deoxyurdine (EdU) incorporation were used to determine the role of HA in maintaining slow-cycling and proliferating cells within the MG, respectively. Data were confirmed using an in vitro proliferation assay, differentiation assay and spheroid cultures.

Results. *Has* knockout mice present precocious MG development, and adult mice present MG hyperplasia and dysmorphic MGs and eyelids, with hyperplastic growths arising from the palpebral conjunctiva. Our data show that a highly organized HA network encompasses the MG, and basal cells are embedded within this HA matrix, which supports the proliferating cells. Spheroid cultures showed that HA promotes acini formation.

Conclusions. HA plays an important role in MG and eyelid development. Our findings suggest that *Has* knockout mice have abnormal HA synthesis, which in turn leads to precocious and exacerbated MG morphogenesis culminating in dysmorphic eyelids and MGs.

Keywords: extracellular matrix, hyaluronan, Meibomian gland, development, stem cells

The tear film plays a vital role in maintaining a healthy ocular surface, including reducing the risk of infection. It is composed of three layers, including a lipid layer, an aqueous layer, and a mucin layer, and each layer plays a fundamental role in tear film function. The outer lipid layer is required to reduce evaporation of the remaining layers. The aqueous layer is the middle layer and is primarily responsible for lubricating the ocular surface, washing away foreign particles, and preventing infection. Finally, the mucin layer lies immediately over the cornea and helps to evenly distribute the aqueous layer and keep it adhered to the ocular surface. The lipid layer is produced by the Meibomian gland (MG), which is located within the tarsal plate in both the upper and lower eyelids.[1] MGs contain secretory acinar cells connected to a central duct that opens onto a mucocutaneous junction at the lid margin. Macroscopically, the acinar lobules flanking the central duct are distinctly visible as yellow. The meibum is secreted by terminally differentiated meibocytes and collects in the central duct through which it is delivered to the ocular surface.[2,3] Like sebaceous glands, MGs are holocrine glands, which means that they discharge the secreting cells in their entirety. As such, meibocytes synthesize and accumulate lipids, becoming terminally differentiated, after which they move centripetally toward the center of an acinus and undergo degeneration and disintegration as they discharge secretions.[4] This lifelong differentiation and destruction of acinar cells require continual turnover of the basal layer. It has been suggested that a reservoir of progenitor cells, or slow-cycling stem cells, would have to exist within MGs to provide long-term renewal of acinar cells,[5] similar to what is seen in hair follicles,[6,7] and other exocrine glands, such as mammary gland,[8] lacrimal glands,[9] and salivary glands.[10]

Changes to MGs that lead to a reduction or alteration in lipid quality/content may lead to a common ocular surface disorder, MG dysfunction (MGD).[11] Alterations in the lipid content of the outer lipid layer lead to an unstable tear film and increased evaporation of the aqueous layer. MGD is a major cause of evaporative dry eye disease, with prevalence ranging from 39% to 50% in the United States.[12] Factors that influence the development of MGD are age and gender, with an increased prevalence seen in women.[11–14] The use of contact lenses in low humidity environments is also a risk factor for MGD.[15] The use of some prescription medications such as isotretinoin and severe cases of *Demodex brevis* mite infestation may lead to the onset of MGD.[16,17] Elucidating the mechanisms that govern healthy development and homeostasis of the MG are of vital importance to understand the pathological processes that lead to MGD.

Hyaluronan (HA) is a nonsulfated glycosaminoglycan composed entirely of repeating disaccharides of glucuronic acid and

N-acetylglucosamine, which are alternately linked by β-1,3- and β-1,4-glycosidic bonds.[18,19] HA is a ubiquitous component of the extracellular matrix (ECM) and is responsible for approximately 3% of the human dry body weight. HA plays an integral role in maintaining tissue integrity and homeostasis, development, inflammation, tissue repair, and wound healing.[20–24] Alterations in HA expression have been shown to lead to age-related pathologies, such as arthritis and tumorigenesis.[25,26] We have recently shown that HA matrices are present within stem cell niches and play an important role supporting stem cells.[27–29] HA is present in tissues in primarily two forms: high molecular weight HA (HMWHA) of approximately 2000 kDa and low molecular weight HA (LMWHA) of approximately 200 kDa. These two forms of HA have drastically distinct physiologic functions and, therefore, the size of the HA chains dictates the composition and function of specific HA matrices that are formed. HMWHA is primarily correlated with development, homeostasis, and tissue integrity, whereas LMWHA is primarily correlated with tissue remodeling and pathogenesis. Therefore, targeting the HA content during pathogenesis, including injury, inflammatory disorders, cardiovascular disease, and cancer, is becoming an extremely attractive strategy for intervention.[25,30,31] HA is naturally synthesized by HA synthases (HASs), of which vertebrates have three isoforms: HAS1, HAS2, and HAS3.[32,33] The mechanism by which HAS enzymes regulate the length of the growing HA chain during the biosynthetic process, which could explain the evolutionary pressure for mammals to express three HAS isoforms, remains to be established.[34] It has been speculated that HAS1 and HAS2 produce primarily HMWHA, whereas HAS3 produces primarily LMWHA; however, some groups have shown that all HAS isoforms have the ability to make both HMWHA and LMWHA.[35,36] Interestingly, naked mole rat (*Heterocephalus glaber*) fibroblasts have been shown to secrete extremely-high molecular weight HA (EHMWHA), over five times higher than that found in other mammals including humans.[37] This EHMWHA contributes to the exceptionally high longevity and unusual resistance to cancer displayed by naked mole rats.

MGs and hair follicles share similar developmental cues.[38,39] Similar to hair follicles, MGs are formed by epithelial-mesenchymal interactions that lead to the invagination of epithelial cells into the mesenchymal tissue. Intricate ECM-cell interactions regulate epithelial cell invagination and proliferation into the eyelid. Importantly, as with other skin appendages, the ECM must be digested at the tip of the developing MG to allow for its ingrowth into the mesenchymal tissue. Previous studies have demonstrated the important role HA plays in the skin development and skin appendage formation.[40–43] Unpublished findings made during a previous study revealed that the tarsal plate was an HA-rich tissue.[29] The ECM-MG interplay that governs the development of the MG remains elusive. Given the important role HA plays in morphogenesis and the lack of information regarding the role of the ECM in MG development, we hereby investigated the role of HA in eyelid formation and MG development and function.

Materials and Methods

Animal Maintenance

Mouse Strains and Genotyping. Mouse models were generated to knock out the HASs: *Has1* and *Has3* null mice were bred to generate $HAS1^{-/-}$;$HAS3^{-/-}$ mice and $HAS2^{flox/flox}$ mice were bred with K14-rtTA (stock number 008099; The Jackson Laboratory, Bar Harbor, ME, USA) and tetO-cre (stock number 006224; The Jackson Laboratory) to generate compound K14-rtTA, tetO-cre (TC), and *Has2flox/flox* that lack *Has2* in the MG, namely $HAS2^{\Delta/\Delta MG}$.[29,44–47] K14-rtTA was selected to induce the excision of *Has2* in the eyelid and MG, because MG abnormalities were noted during our previous studies using these mice.[29] Administration of doxycycline chow was used to induce K14-driven persistent and irreversible excision of *Has2* in the MG of triple-transgenic mice (K14-rtTA;TC; $HAS2^{flox/flox}$), generating $HAS2^{\Delta/\Delta MG}$.[48] The mice were housed in a temperature-controlled facility with an automatic 12-hour light-dark cycle at the Animal Facility of the University of Houston. Experimental procedures for handling the mice were approved by the Institutional Animal Care and Use Committee, University of Houston. K5tTA mice were kindly provided by Adam Glick[49] and were bred with H2B-GFP mice (The Jackson Laboratory) to generate bigenic mice with green fluorescent protein (GFP) expression in keratin 5 (K5) expressing cells regulated by doxycycline administration (tet-off). H2B-GFP/K5tTA mice were maintained at Heath Park Animal Facility, Cardiff University and bred under protocol 3 of project license number (PPL) 30/3022. The use of animals in experiments in the United Kingdom is regulated under the Animals (Scientific Procedures) Act 1986. All animal procedures adhered to the ARVO Statement for the Use of Animals in Ophthalmic and Vision Research. The identification of each transgene allele was determined by PCR genotyping with tail DNA.

Administration of Doxycycline to Induce Conditional Knockout of *HAS2* in the MG and Induce GFP Expression in H2B-GFP/K5tTA Mice

Doxycycline chow was fed to $HAS2^{\Delta/\Delta MG}$ mice in order to induce K14-driven persistent and irreversible excision of *Has2* in $K14^{+}$ cells, which would include the MGs. The mice for this study were induced at embryonic day 0 (E0). Transgenic mice including the pregnant dams were fed with doxycycline chow (1 g of doxycycline/kg of chow; Custom Animal Diets LLC, Bangor, PA, USA). For such, the female mice were placed on doxycycline chow upon mating ad libitum in lieu of regular chow (Dox diet catalog no. AD3008S; Custom Animal Diets, Bangor, PA, USA) and kept on this special diet through to weaning, and, thereafter, the weaned mice were maintained on doxycycline chow. Mice lacking either the K14-rtTA or tetO-cre allele were also supplied with doxycycline chow and used as littermate controls. H2B-GFP/K5tTA were pulsed from P0 to P28 to label all MG cells with nuclear GFP and then fed doxycycline (2 g/kg) for 28 days chase. K5 cells that divide in the chase phase lose 50% GFP fluorescence, which means that slow-cycling epithelial progenitors can then be identified by their retention of the GFP label.

Tissue Processing During Developmental Stages

Mice were euthanized with CO_2 and heads collected at postnatal days (PDs) 0, 1, 5, and 12, eyelids were collected at PD26 or from adult mice (7–8 weeks old), and tissues were immediately fixed in 4% paraformaldehyde at 4°C. The next day, the tissues were washed with PBS. For whole-mount staining, the eyelids were dissected and processed for whole mount. At least 15 samples were analyzed for whole-mount staining per experimental point. For histology, the eyelids were embedded in tissue freezing medium and processed for cryosectioning. At least five samples were analyzed per experimental point. Both male and female mice were used in the study, yielding comparable results.

Oil Red O Staining

The eyelids were immersed in oil red O solution (Sigma-Aldrich Corp., St. Louis, MO, USA) that stains neutral triglycerides and lipids, and were left under gentle agitation at room temperature for 1 (pup eyelids) or 2 (adult eyelids) hours, protected from light. The eyelids were then destained by gently rinsing with deionized water. The eyelids were then mounted and imaged.

Whole-Mount Staining

The eyelids or tarsal plates were incubated in permeabilization buffer (0.25% dimethyl sulfoxide [DMSO], 0.25% Triton X-100, and 15% sucrose in PBS) for 30 minutes at room temperature under constant rotation and rinsed with PBS. Thereafter, the eyelids were stained with Alexa-546 Phalloidin (Thermo Fisher Scientific, Wilmington, DE, USA) and 4′,6-diamidino-2-phenylindole (DAPI; Sigma-Aldrich Corp.) in staining buffer (0.25% DMSO, 0.01% saponin, and 15% sucrose in PBS) overnight under constant rotation at 4°C protected from light. Tarsal plates were stained with biotinylated HA binding protein (HABP-385911; Millipore, Billerica, MA, USA) in staining buffer (0.25% DMSO, 0.01% saponin, and 15% sucrose in PBS) overnight under constant rotation at 4°C followed by incubation of the NeutrAvidin Alexa Fluor 555 conjugate overnight under constant rotation at 4°C protected from light. The eyelids and tarsal plates were washed with staining buffer followed by PBS and mounted on glass slides in Fluoromount-G (SouthernBiotech., Birmingham, AL, USA). The eyelids were imaged using an LSM 800 confocal microscope with Axiocam 503 color (Zeiss, Oberkochen, Germany). For analyzing the distribution of HA matrices, the tarsal plate whole mounts were imaged with Aryscan by using the 63× objective.

Stereomicroscope Imaging

The eyelids were trimmed under a dissecting microscope for them to be mounted as flat mounts with the MGs exposed. During the dissections, the lateral and medial canthus were opened with a pair of microsurgical scissors and excess skin was removed. Images were acquired of stained and unstained eyelids by using a fluorescence stereomicroscope Discovery.V12 with an Axiocam 503 color (Zeiss).

Immunohistochemistry

Eyelids were collected and immediately fixed in 4% buffered paraformaldehyde overnight and then embedded in Tissue-Tek embedding medium (Sakura Finetek USA, Inc., Torrance, CA, USA) for cryosectioning. Sections (10 μm) were cut using a Leica CM 1950 (Leica, Buffalo Grove, IL, USA) cryostat and collected on Fisherbrand SuperfrostPlus Gold microscope slides (Thermo Fisher Scientific). Upon use, sections were incubated for 30 minutes at 60°C, and excess tissue embedding medium was removed with PBS. Unspecific protein binding sites were blocked with 10% fetal bovine serum (FBS) prepared in PBS containing 0.01 M saponin. Sections were then incubated with the primary antibodies anti-Krt14 (PRB-155P; Covance, Princeton, NJ, USA) and HA binding protein (Millipore). Sections were washed and incubated with NeutrAvidin Alexa Fluor 555 conjugate and anti-rabbit produced in donkey conjugated with Alexa 488 for 1 hour at room temperature. A secondary control was carried out with rabbit IgG isotype control (Abcam, Cambridge MA, USA) in place of the primary antibody and did not yield any staining (results not shown). Slides were mounted in Fluoromount-G and imaged under an LSM 800 confocal microscope (Zeiss).

RNA Extraction From MGs and Real-Time PCR Analysis

Eyelids were obtained from adult mice and the tarsal plate containing the MG were isolated under a stereomicroscope and snap frozen in liquid nitrogen. Total RNA was isolated from the MGs by using Trizol Reagent (Invitrogen, Carlsbad, CA, USA). Upon isolation, the RNA concentration and purity were determined using a spectrophotometer at 260 and 280 nm. First strand cDNA was reverse transcribed using 2 μg of total RNA and the high capacity cDNA Reverse Transcription kit (Catalog no. 4368814, lot 00593854; Applied Biosystems, Lithuania), according to the manufacturer's protocol. Quantitative real-time PCR amplification was performed on 1 μl or 50 ng of the cDNA (1:5) with specific primers for *Has* 1–3, β-actin (*Actb*), and *Gapdh* and the kit Powerup SYBR Green Master Mix (Catalog no. A25918; Applied Biosystems) in a CXF Connect Realtime System from Bio-Rad Laboratories (Bio-rad, Hercules, CA, USA) by using the activation cycle of 95°C for 10 minutes, 40 cycles of 95°C for 15 seconds and 60°C for 1 minute. The specificity of the amplified products was analyzed through dissociation curves generated by the equipment, yielding single peaks. Negative controls were used in parallel to confirm the absence of any form of contamination in the reaction. Analysis of the data was carried out using the $2^{-\Delta Ct}$ methods for the $HAS1^{-/-}$;$HAS3^{-/-}$ samples and the $2^{-\Delta\Delta Ct}$ method for the $HAS^{\Delta/\Delta MG}$ samples by using the CXF Connect Realtime System's software and Microsoft Office 10 excel. The primer combination used for *Has1* was forward 5′-CTATGC TACCAAGTATACCTCG-3′ and reverse 5′-TCTCGGAAGTAA GATTTGGAC-3′; for *Has2* was forward 5′-CGGTCGTCTCA AATTCATCTG-3′ and reverse 5′-ACAATGCATCTT GTTCAGCTC-3′; for *Has3* was forward 5′-GATGTC CAAATCCTCAACAAG-3′ and reverse 5′-CCCACTAATACATTG CACAC-3′; for *Actb* was forward 5′-CACTGTCGAGTCGCGTCC -3′ and reverse 5′-TCATCCATGGCGAACTGGTG-3′; and for *Gapdh* was forward 5′-AACAGCAACTCCCACTCTTC-3′ and reverse 5′-CCTGTTGCTGTAGCCGTATT-3′. MGs were isolated from three $HAS1^{-/-}$;$HAS3^{-/-}$ and wildtype (wt) mice and five $HAS^{\Delta/\Delta MG}$ mice. MGs were isolated from the left and right, upper and lower eyelids, and pooled for each individual animal. The expression profile of each individual animal was analyzed independently and presented as a single point in the graphs.

In Vivo Cell Proliferation Assay

To verify whether HA regulates the proliferation of MG epithelial cells, we injected adult mice with EdU so that cells actively dividing would incorporate EdU into their newly synthesized DNA (Life Technologies, Eugene, OR, USA). Mice were labeled with 200 μg EdU/g body weight by intraperitoneal injection for 6 hours. Thereafter, the mice were euthanized by CO_2 inhalation and their eyelids collected and fixed in 4% buffered paraformaldehyde overnight. The eyelids were processed for cryosectioning or tarsal plate whole-mount staining. Sections (10 μm) were cut and collected, as mentioned above. The incorporated EdU was developed using the Click-IT Alexa Fluor 488 kit (Life Technologies, Carlsbad, CA, USA) to reveal the incorporated EdU. The sections or whole-mount eyelids were then counterstained with HA and DAPI, as described above and mounted in Fluoromount-G. Images were captured using an LSM 800 confocal microscope.

MG Epithelial Cells

Immortalized human MG epithelial cells (hMGCs) were kindly provided by David Sullivan and cultured as previously

described.[50] In short, hMGCs were maintained in keratinocyte serum-free medium containing 5 ng/mL epidermal growth factor (EGF) and 50 μg/mL bovine pituitary extract (Invitrogen). Experiments were carried out with cells between passages 5 and 7.

In vitro Proliferation Assay

The effect of HA on MG cell proliferation was assayed in vitro by measuring the incorporation of 5-bromo-2-deoxyuridine (BrdU) into the newly synthesized DNA of replicating cells (BrdU Cell Proliferation Kit, EMD Millipore, Darmstadt, Germany). The hMGCs were plated at a seeding density of 5000 cells/well in 96-well plates and allowed to grow for 24 hours in the presence or absence of HA or 4-methylumbelliferone (4-MU; Sigma-Aldrich Corp.). The concentrations used were 0.02% and 0.05% of HMWHA; 0.02% and 0.05% of LMWHA; or 0.25 mM, 0.5 mM, or 2 mM of 4-MU. After 24 hours, with the cells in their exponential growth phase, BrdU was added to each well and left for 2 hours. The cells were then fixed and the detection of BrdU incorporation carried out according to the manufacturers' instructions. Absorbance in each well was read as optical density (OD) by using a spectrophotometer microplate reader (Fluostar Omega, BMG Labtech, Offenburg, Germany) set at a test wavelength of 450 nm. Each condition was tested in triplicate and three separate experiments were carried out. The mean of each individual experiment is presented as a single point on the graph.

Hanging Drop 3D Culture System

In order to further study the role of HA on MG development, the 3D hanging drop culture system was used. Ten-microliter drops of hMGCs at a density of 2.5×10^4 cells/mL were placed on the inside of a 60-mm petri dish lid (Eppendorf, Hauppauge, NY, USA). Various brands were tested, and the Eppendorf-treated cell culture dishes presented the highest surface tension and were, therefore, the most suitable for the hanging drop technique. The hMGCs were placed in culture in the presence or absence of HA, specifically 0.01% ULMWHA, 0.05% LMWHA and 0.05% HMWHA were used. The lids were then inverted and placed over a petri dish containing 1 mL PBS to prevent the drops from drying out. On day 4, FBS at a final concentration of 10% was added to the cells to trigger differentiation, and the cultures were maintained for a further 6 days. The cells were maintained at 37°C and 5% CO_2 for a total of 10 days after which images were taken and the spheres were fixed in 2% paraformaldehyde for 30 minutes. The spheres were washed with PBS, blocked, and stained with Alexa Fluor 488 Phalloidin (Cell Signaling, Eugene, OR, USA) and HA binding protein (Millipore) followed by NeutrAvidin Alexa Fluor 555 conjugate. Nuclei were counterstained with DAPI.

MG Epithelial Differentiation Assay

Previous studies have shown that the hMGCs used in this study remain progenitor-like when maintained in serum-free media. However, when FBS is added to the media, the cells terminally differentiate and start to accumulate lipid droplets within the cytoplasm. In order to verify whether HA regulates MG cell differentiation and lipid production, hMGCs were stimulated with FBS in the presence or absence of HA and lipid levels were measured using HCS LipidTOX Red neutral lipid stain (Invitrogen). The effect of HA on hMGCs differentiation was assayed by either adding HMWHA, LMWHA, or 4-MU to the media, or coating the dish with poly-D-lysine (PDL) followed by HMWHA (Lifecore Biomedical, Chaska, MN, USA) or LMWHA (Lifecore Biomedical). For assaying the effect of soluble HA, hMGCs were cultured in keratinocyte serum-free medium (Invitrogen) containing 5 ng/mL EGF and 50 μg/mL bovine pituitary extract. When cells reached approximately 70% to 80% confluence, the media was replaced with Dulbecco's modified Eagle's medium and Ham's F12 (1:1) containing 10 ng/mL EGF and 10% FBS supplemented or not with 0.05% HMWHA, 0.05% LMWHA, or 0.5 Mm 4-MU. When lipid droplets were evident within the cytoplasm of the control cells, LipidTOX was added to the media and left for 24 hours, after which the cells were imaged and fixed with 4% paraformaldehyde. For assaying the effect of an HA substrate on differentiation and lipid production, culture dishes were treated with PDL (20 ug/mL) for 2 hours at room temperature, followed by 0.1% HMWHA or 0.1% LMWHA overnight at 4°C. Thereafter, MGCs were seeded on the coated plates and cultured in Ham's F12 (1:1) containing 10 ng/mL EGF and 10% FBS keratinocyte serum-free medium (Invitrogen) containing 5 ng/mL EGF and 50 μg/mL bovine pituitary extract. Controls were carried out with PDL-coated dishes and uncoated dishes. When lipid droplets were evident within the cytoplasm of the control cells, LipidTOX was added to the media and left for 24 hours, after which the cells were imaged and fixed with 4% paraformaldehyde. The experiments were carried out in sextuplicate and repeated twice. A total of 25 images were captured for each experimental group and the number and size of lipid droplets graded by two individual investigators in a blinded manner.

Statistics

All values are presented as standard deviation of the mean. The difference between two groups was compared by Student's *t*-test and between more than two groups by 1-way ANOVA. Values with $P \leq 0.05$ were considered to be statistically significant. Statistical analysis was performed using the GraphPad Prism version 5 software package (GraphPad Software, San Diego, CA, USA).

Results

Has Knockout Mice Present Altered MGs

Eyelids were obtained from $HAS1^{-/-}$;$HAS3^{-/-}$, $HAS2^{\Delta/\Delta MG}$, and wt adult mice stained with oil red O and analyzed under a stereomicroscope (Fig. 1). The MGs of $HAS1^{-/-}$;$HAS3^{-/-}$ and $HAS2^{\Delta/\Delta MG}$ mice were found to be enlarged, elongated, and contained a larger lipid volume when compared with wt mice (Fig. 1).

Histologic Analysis of MGs From $HAS1^{-/-}$;$HAS3^{-/-}$, $HAS2^{\Delta/\Delta MG}$, and Wt Mice

Eyelids were obtained from $HAS1^{-/-}$;$HAS3^{-/-}$, $HAS2^{\Delta/\Delta MG}$, and wt adult mice, processed for histology, and sagittal (Fig. 2) cryosections were prepared. The expression of HA and K14 were analyzed in the tissues (Fig. 2). K14 is an intermediate filament that is present in the cytoskeleton of cells of epithelial origin. The development of the MG relies on developmental cues triggered by epithelial-mesenchymal interactions that lead to the invagination of epithelial cells into the mesenchymal tissue. Thus, in the eyelid, epithelial cells and cells of epithelial origin, such as the MG and hair follicles, all express K14. K14 was therefore used in this study to outline the MGs and also as an indication as to which cells would lack *Has2* in $HAS2^{\Delta/\Delta MG}$ mice, because K14-rtTA was used to drive the excision of *Has2*. K14 staining confirmed that $HAS1^{-/-}$;$HAS3^{-/-}$ and

Investigative Ophthalmology & Visual Science

Figure 1. Whole eyelids were obtained from wt, *HAS1*$^{-/-}$;*HAS3*$^{-/-}$, and *HAS2*$^{\Delta/\Delta MG}$ adult mice, fixed, trimmed, and mounted to enable flat mount. Images were captured under a stereomicroscope (*top panel*). After imaging, the eyelids were stained with oil red O solution and then mounted and imaged under a stereomicroscope using white light (*middle panel*) and the 555 channel (*lower panel*). *Scale bar*: 250 μm.

HAS2$^{\Delta/\Delta MG}$ mice present larger MGs compared with wt mice (Fig. 2). Moreover, *HAS1*$^{-/-}$;*HAS3*$^{-/-}$ and *HAS2*$^{\Delta/\Delta MG}$ mice present dysmorphic MGs, which are no longer elongated in shape, with a larger number of meibocytes per acinus (Fig. 3A). Wt mice present an average of 12 meibocytes per acinus in a single plane, whereas *HAS1*$^{-/-}$;*HAS3*$^{-/-}$ mice present 19.5 and *HAS2*$^{\Delta/\Delta MG}$ mice present 20. Based on the HA staining pattern of eyelids of wt mice, HA is expressed in eyelids primarily by tissues of mesenchymal origin. In Figure 2, a white dashed line was used to outline the eyelid and MG. Strong HA expression was seen circumventing MG acini, whereas low HA expression was detected within MG cells (Fig. 2). We did not observe a significant change in the HA staining pattern between eyelids of knockout mice when compared with wt mice. However, based on the HA staining, *HAS1*$^{-/-}$;*HAS3*$^{-/-}$ and *HAS2*$^{\Delta/\Delta MG}$ mice do not present a decrease in HA expression in eyelids (Fig. 2).

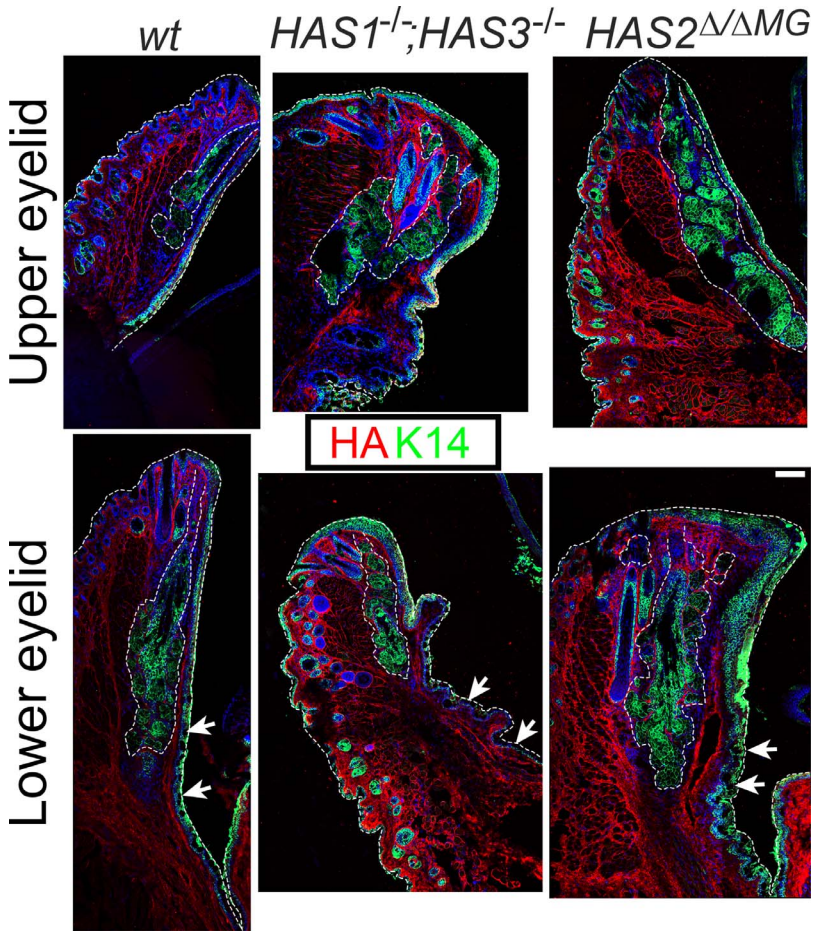

Figure 2. HA (*red*) and K14 (*green*) staining in sagittal sections of adult eyelids from wt, *HAS1*$^{-/-}$;*HAS3*$^{-/-}$, and *HAS2*$^{\Delta/\Delta MG}$ adult mice. Staining revealed that HA is present throughout the eyelid primarily in tissues of mesenchymal origin. In the MG, HA is present surrounding the acinar basal cells throughout the gland and also along the central collecting duct. The upper eyelid is shown in the *top panel* and the lower eyelid in the *bottom panel*. A *white dashed line* was used to outline the MG and the eyelid. *White arrows* indicate the palpebral conjunctiva. Nuclei were counterstained with DAPI (*blue*). *Scale bar*: 100 μm.

Investigative Ophthalmology & Visual Science

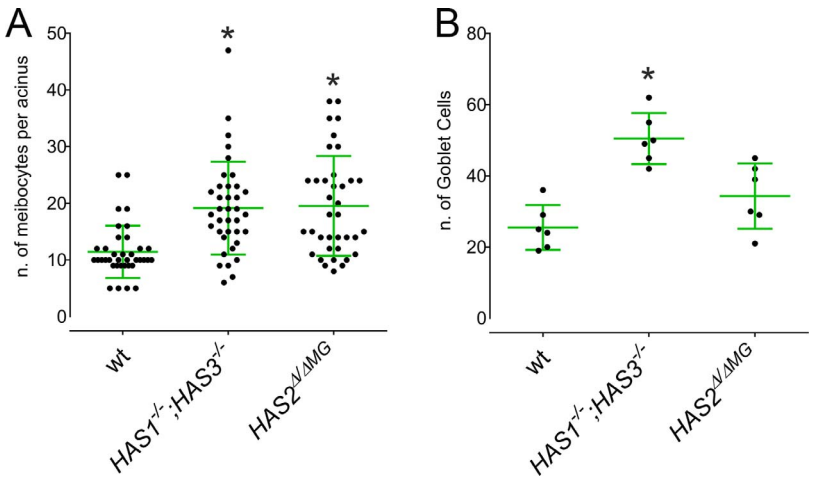

Figure 3. The number of meibocytes and goblet cells in wt, *HAS1*$^{-/-}$;*HAS3*$^{-/-}$, and *HAS2*$^{\Delta/\Delta MG}$ adult mice. The number of meibocytes present in a single plane of an acinus of wt, *HAS1*$^{-/-}$;*HAS3*$^{-/-}$, and *HAS2*$^{\Delta/\Delta MG}$ adult mouse MGs was counted in a double blinded manner (**A**). The number of goblet cells present along the palpebral conjunctiva in a single plane of wt, *HAS1*$^{-/-}$;*HAS3*$^{-/-}$, and *HAS2*$^{\Delta/\Delta MG}$ adult mouse eyelids was counted in a double blinded manner (**B**). $^{*}P \leq 0.05$.

HA Distribution in the MG and Tarsal Plate

Given that HA is highly expressed surrounding the MG and tarsal plate, we investigated the organization of the HA matrices in these tissues. The distribution and organization of the HA network was analyzed in tarsal plate whole mounts of *HAS1*$^{-/-}$;*HAS3*$^{-/-}$, *HAS2*$^{\Delta/\Delta MG}$, and wt mice. Interestingly, HA forms distinct matrices in the tarsal plate and surrounding the MB. The whole-mount analysis revealed that HA forms an intricate 3D HA network surrounding the basal cells of the MG, with geometry resembling chain-link woven netting (Fig. 4, lower panel), as previously shown.[51] However, in the tarsal plate HA forms cable-like structures (Fig. 4, upper panel), as previously shown.[27]

HAS Knockout Mice Present Dysmorphic Eyelids With Epithelial Hyperplasia

HAS1$^{-/-}$;*HAS3*$^{-/-}$ and *HAS2*$^{\Delta/\Delta MG}$ mice present dysmorphic eyelids. The mice present epithelial hyperplasia leading to hyperplastic growths arising from the palpebral conjunctival epithelium, causing the development of prominent papules or nodules. The hyperplastic outgrowths were present along the palpebral conjunctival epithelium of all *HAS1*$^{-/-}$;*HAS3*$^{-/-}$ and *HAS2*$^{\Delta/\Delta MG}$ mice, leading to a loss of the smooth wiping surface of the eyelids (Fig. 2). Due to the outgrowths on the inner surface of the eyelids, *HAS1*$^{-/-}$;*HAS3*$^{-/-}$ and *HAS2*$^{\Delta/\Delta MG}$ mice present an increase in conjunctival surface area, including an increase in the number of goblet cells (Fig. 2, white arrow). *HAS1*$^{-/-}$;*HAS3*$^{-/-}$ mice present a 2-fold increase

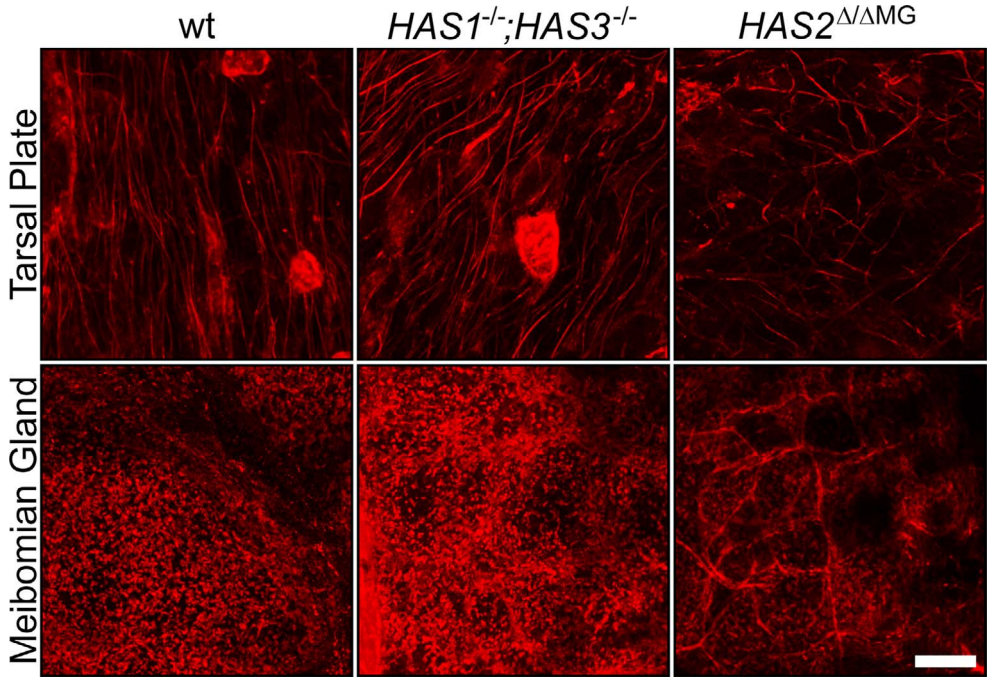

Figure 4. The organization of HA (*red*) was analyzed in wt, *HAS1*$^{-/-}$;*HAS3*$^{-/-}$, and *HAS2*$^{\Delta/\Delta MG}$ adult mouse tarsal plate whole mounts. Nuclei were counterstained with DAPI (*blue*). *Scale bar*: 10 μm.

Investigative Ophthalmology & Visual Science

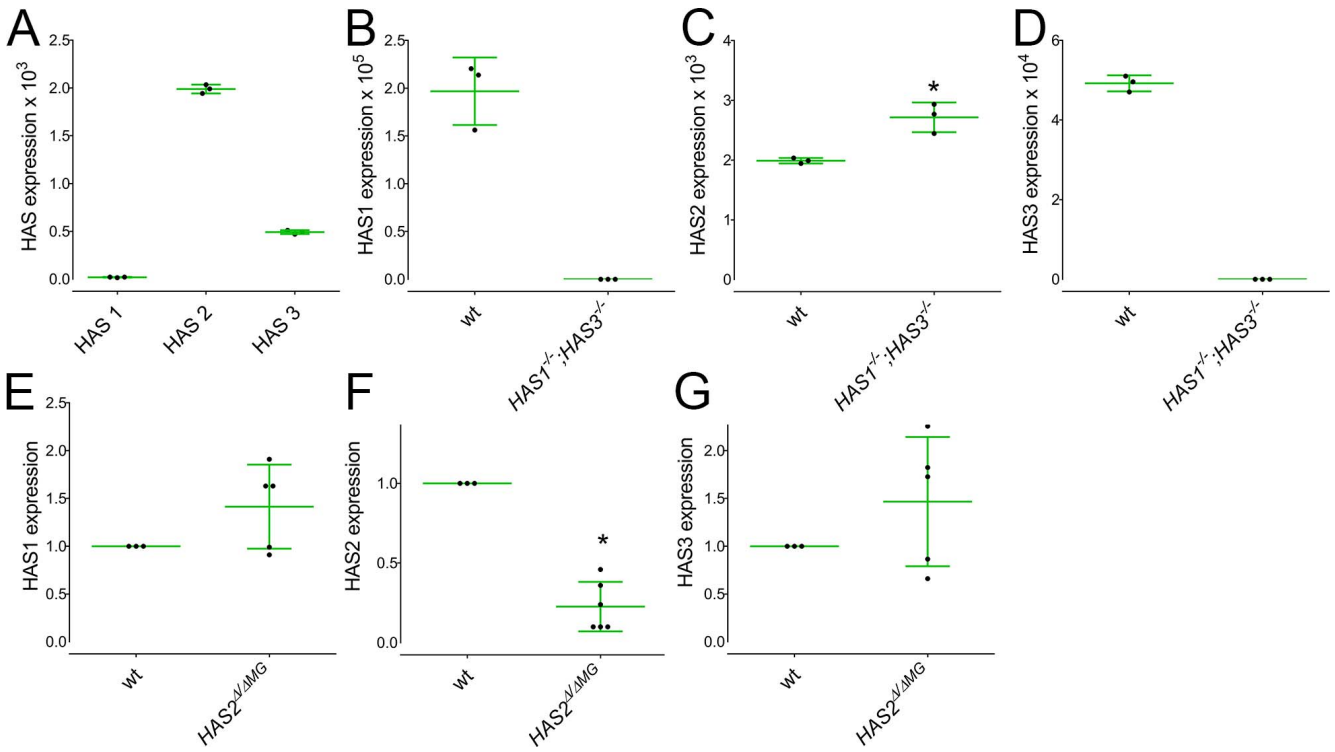

Figure 5. The expression profile of *Has 1–3* in the MG were analyzed by real-time PCR. RNA was isolated from the MGs of wt (**A–G**) *HAS1*$^{-/-}$;*HAS3*$^{-/-}$(**B–D**), and *HAS2*$^{\Delta/\Delta MG}$ mice (**E–G**) and the expression levels of *Has1*, *2*, and *3* were quantified. Error bars present standard deviation. $^{*}P \leq 0.05$.

in the number of goblet cells when compared with wt mice (Fig. 3B). Curiously, the tet-off H2B-GFP/K5tTA mice revealed that the slow-cycling epithelial cells of the palpebral conjunctiva also lie within an HA matrix (results not shown). Thus, HA could also play a role in regulating the epithelial stem cells of the palpebral conjunctiva, and changes in HA lead to an increase in cell proliferation.

Analysis of the Expression Profile of *Hass* in the MGs of *HAS1*$^{-/-}$;*HAS3*$^{-/-}$, *HAS2*$^{\Delta/\Delta MG}$, and Wt Mice

Due to the fact that mice lacking the HAS enzymes did not present a loss of HA surrounding the MGs, we investigated the expression profile of the different *Hass* to verify if *HAS1*$^{-/-}$;*HAS3*$^{-/-}$ upregulates *Has2* and *HAS2*$^{\Delta/\Delta MG}$ upregulates *Has1* and/or *3* through a compensatory mechanism. For such, eyelids were obtained from *HAS1*$^{-/-}$;*HAS3*$^{-/-}$, *HAS2*$^{\Delta/\Delta MG}$, and wt adult mice and the tarsal plates dissected for RNA extraction. The expression profiles of *Has1–3* were analyzed by real-time PCR (Fig. 5). Interestingly, *Has1–3* are expressed in the MB, with *Has2* being the most highly expressed of the synthases and *Has*1 the least expressed (Fig. 5A). *HAS1*$^{-/-}$;*HAS3*$^{-/-}$ mice present an upregulation *Has2* when compared with the wt mice, thereby compensating for the loss of *Has1* and *Has3* (Fig. 5C). The lack of *Has1* and *Has3* expression was confirmed in the *HAS1*$^{-/-}$;*HAS3*$^{-/-}$ mice (Figs. 5B, 5D). *HAS2*$^{\Delta/\Delta MG}$ mice presented a significant reduction of *Has2* expression, to 25% of that of wt mice, and therefore confirming the loss of *Has2* in the MGs of *HAS2*$^{\Delta/\Delta MG}$ mice (Fig. 5F). *HAS2*$^{\Delta/\Delta MG}$ mice upregulate the expression of *Has1* and/or *3* in the MGs (Figs. 5E–G). Curiously, of the five mice analyzed, two *HAS2*$^{\Delta/\Delta MG}$ mice upregulated solely *Has1* expression, two mice upregulated solely *Has3* expression, and one mouse upregulated both *Has1* and *3* (Figs. 5E–G).

Slow-Cycling MG Progenitor Cells Are Present Within an HA Matrix

Putative stem cell populations have been speculated to exist within the MG, providing a constant supply of new basal cells. Due to the lack of well-characterized stem cell markers for MG stem cells we used tet-off H2B-GFP/K5tTA mice (as previously shown) to verify whether K5 label-retaining cells (LRCs), which are slow-cycling progenitor cells, are localized within the HA-rich niches.[5] Although stem cell niches have still to be identified within the MG, slow-cycling progenitor cells (H2B-GFP^{+} LRCs) have been shown to be present within the MG ductule that terminates at each acinus by using H2B-GFP/K5tTA mice after pulse/chase labeling.[5] To visualize slow-cycling epithelial progenitors, eyelids were obtained from H2B-GFP/K5tTA adult mice and the tarsal plate processed for whole mount. HA staining revealed that H2B-GFP^{+} LRCs (28-day chase) within the MG were embedded within in an HA matrix (Fig. 6B). Moreover, the whole mount analysis of the tarsal plate confirmed that HA forms an intricate 3D HA network surrounding the MG acini, with geometry resembling chain-link woven netting (Fig. 6B), as previously shown.[51]

Role of HA During MG Morphogenesis

To investigate how changes in HA expression could lead to altered MGs in adult *HAS1*$^{-/-}$;*HAS3*$^{-/-}$ and *HAS2*$^{\Delta/\Delta MG}$ mice, we investigated the morphology of the MGs at different developmental stages. For such, eyelids from P5, P12, and P26 mice were obtained and stained with oil red O and imaged under a stereomicroscope (Fig. 7). In Figure 7, a black dashed box has been used to outline a MG in the wt mice and an equiproportionate box placed over a MG in the *HAS1*$^{-/-}$;*HAS3*$^{-/-}$ and *HAS2*$^{\Delta/\Delta MG}$ mice of the same time-point, to aid in comparing the size of MGs between samples. At P5,

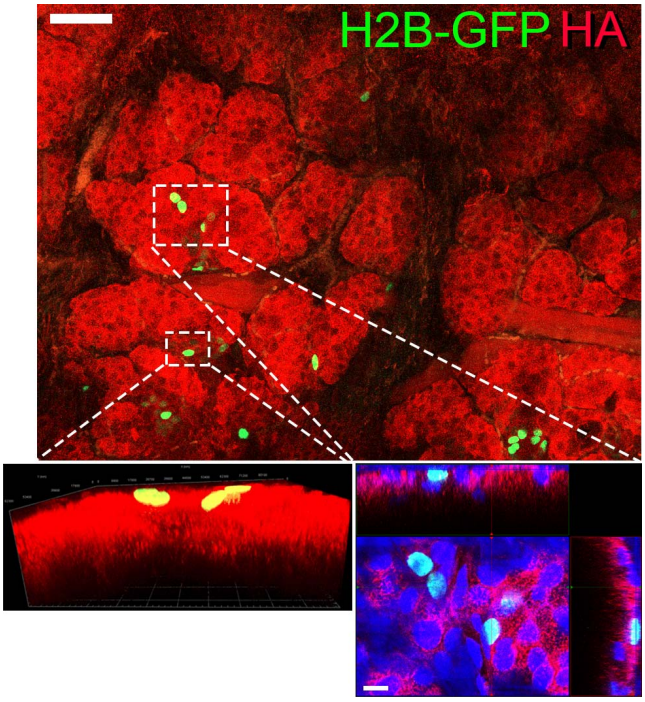

Figure 6. Expression profiles of HA (*red*) and H2B-GFP^{+} cells (*green*) in the MG of adult H2B-GFP/K5tTA mice. In order to verify whether HA could be present in the niche supporting slow-cycling MG progenitor cells, eyelids were obtained from H2B-GFP/K5tTA mice. H2B-GFP^{+} cells (*green*) in the MG were found to be present within an HA matrix (*red*). *Scale bar*: 50 μm (*top image*) or 10 μm (*zoomed image*, cut view).

HAS1$^{-/-}$;*HAS3*$^{-/-}$ mice present longer MGs when compared with wt and *HAS2*$^{\Delta/\Delta MG}$ mice (Fig. 7, top row). At P12, the MGs of *HAS1*$^{-/-}$;*HAS3*$^{-/-}$ and *HAS2*$^{\Delta/\Delta MG}$ mice present more branching and are therefore wider than those of wt mice (Fig. 7, middle row). At P26, the MGs of *HAS1*$^{-/-}$;*HAS3*$^{-/-}$ and *HAS2*$^{\Delta/\Delta MG}$ mice are both longer and wider than those of wt mice, to the extent that there is no gap between the MGs (Fig. 7, bottom row). Therefore, changes in HA expression lead to precocious and excessive MG development.

The role of HA in the development of MGs was also determined by whole-mount immunostaining. Eyelids of P5, P12, and P26 mice were processed for whole mount, stained with phalloidin, and imaged under a confocal microscope evidencing the structure of the MGs (Figs. 8 and 9, MGs are outlined with a white dashed line). The precocious formation of the MGs can be clearly seen in the eyelids of the mice at P5 (Fig. 8). The MGs of wt mice at P5 are cylindrical and do not present any signs of branching at this developmental stage (Fig. 8). On the other hand, both the *HAS1*$^{-/-}$;*HAS3*$^{-/-}$ and *HAS2*$^{\Delta/\Delta MG}$ mice already present branching of the MGs at P5 (Fig. 8). Both the increase in length and width of the MGs at P12 and P26 of *HAS*$^{-/-}$;*HAS3*$^{-/-}$ and *HAS2*$^{\Delta/\Delta MG}$ mice compared with wt mice can also be evidenced by phalloidin staining (Fig. 9). As seen with the images captured with oil red O staining, phalloidin staining evidences that *HAS1*$^{-/-}$;*HAS3*$^{-/-}$ and *HAS2*$^{\Delta/\Delta MG}$ mice lack a gap between the MGs due to the excessive branching that is already evident at P26 (Fig. 9). The distribution of HA in the developing eyelids was also investigated. Histologic sections of P1 eyelids stained with biotinylated HABP revealed that the developing tarsal plate presents strong HA expression (Fig. 10). Thus, the MG develops into an HA-rich tissue. Thus, we speculate that during early stages of MG development, when the epithelial-mesenchymal interaction leads to the invagination of epithelial

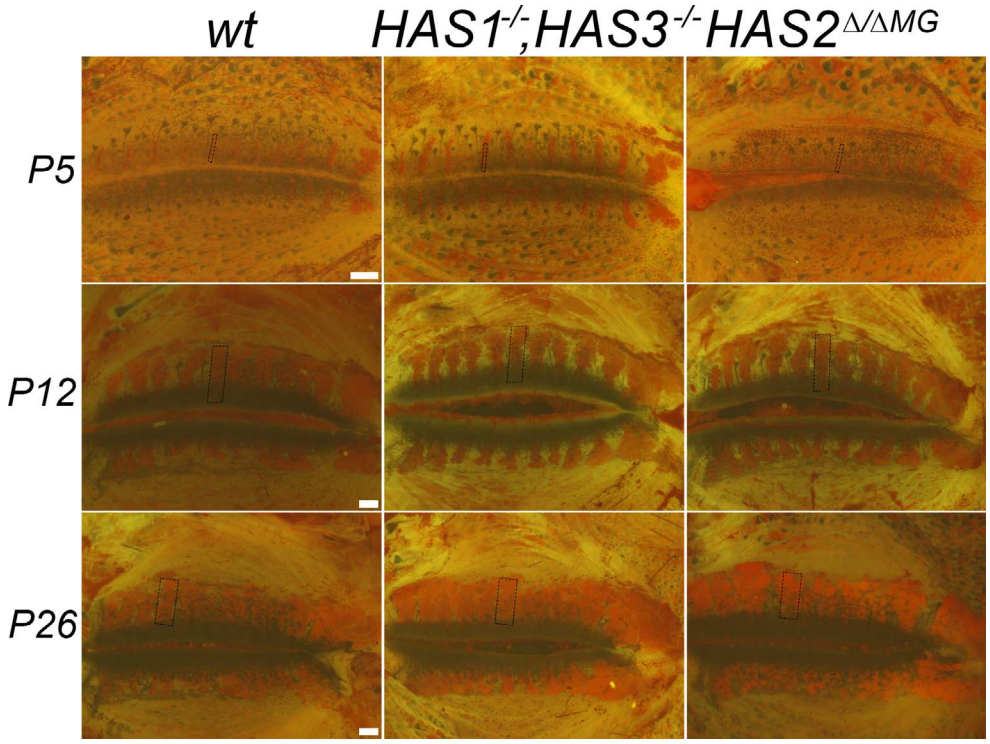

Figure 7. Whole eyelids were obtained from wt, *HAS1*$^{-/-}$;*HAS3*$^{-/-}$, and *HAS2*$^{\Delta/\Delta MG}$ mice at PD5 (*top panel*), PD12 (*middle panel*), and PD26 (*bottom panel*), fixed, trimmed, stained with oil red O, and mounted to enable flat mount. Images were captured under a stereomicroscope. A *black dashed box* has been used to outline a MG in the wt mice and an equiproportionate box placed over a MG in the *HAS1*$^{-/-}$;*HAS3*$^{-/-}$ and *HAS2*$^{\Delta/\Delta MG}$ mice of the same time-point, to aid in comparing the size of MGs between samples. *Scale bar*: 250 μm.

Investigative Ophthalmology & Visual Science

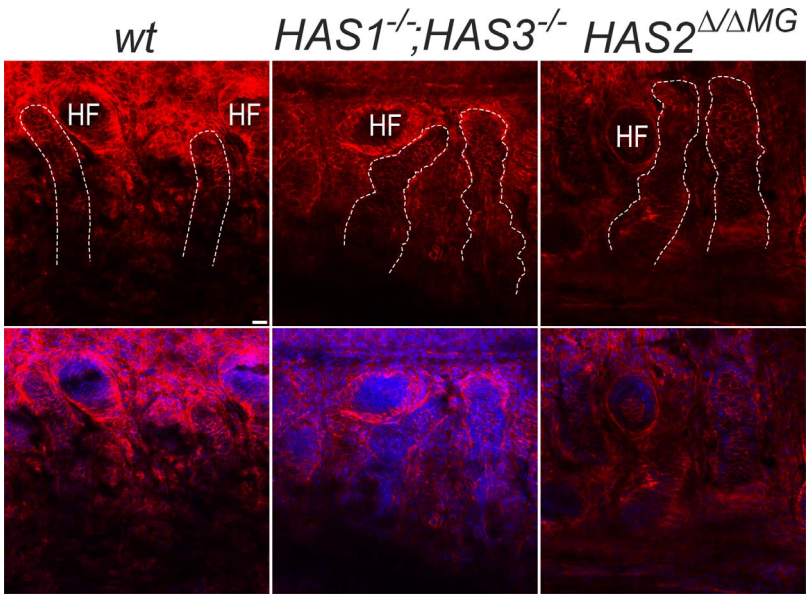

Figure 8. Whole eyelids were obtained from wt, *HAS1*$^{-/-}$;*HAS3*$^{-/-}$, and *HAS2*$^{\Delta/\Delta MG}$ mice at PD5, fixed, trimmed, stained with phalloidin (*red*), and mounted to enable flat mount. Images were captured under a confocal microscope. A *white dashed line* has been used to outline the developing MG. Nuclei were counterstained with DAPI (*blue*). *Scale bar*: 20 μm.

cells into the mesenchymal tissue, the HA-rich mesenchymal tissue could serve as an important cue for regulating the proliferation and inward growth of epithelial cells.

In Vivo and In Vitro Cell Proliferation

Due to the increase in the size of MGs in the knockout mice, we investigated the effect of HA on MG cell proliferation, both in vivo and in vitro. HA in vitro had a stimulatory effect on meibocyte proliferation. Culturing hMGCs in the presence of both HMWHA and LMWHA led to a significant increase in cell proliferation, whereas culturing them in the presence of 4-MU, a chemical inhibitor that specifically blocks the synthesis of HA, led to a significant decrease in cell proliferation and at higher concentrations abrogated cell proliferation (Fig. 11). To assess the effect of HA on MG cell proliferation in vivo, *HAS1*$^{-/-}$;*HAS3*$^{-/-}$, and *HAS2*$^{\Delta/\Delta MG}$, and wt mice were treated with EdU for 6 hours and eyelids were collected and processed for histology and whole-mount immunostaining. The distribution of EdU^{+} cells and HA were analyzed in sagittal sections of the eyelids. An increase in EdU^{+} cells was observed in the *HAS1*$^{-/-}$;*HAS3*$^{-/-}$ and *HAS2*$^{\Delta/\Delta MG}$ mice when compared with control mice (Fig. 12). As described earlier, the basal cells, which are the outer layer of cells that circumvent the MG, are surrounded by an HA-rich matrix. It has been previously shown, as with other holocrine glands, that the acinus of MGs is composed of an outer layer of basal cells that proliferate to generate new meibocytes that gradually move toward the center of the acinus. As the meibocytes move centripetally, they produce and store lipids. As the meibocytes fully mature

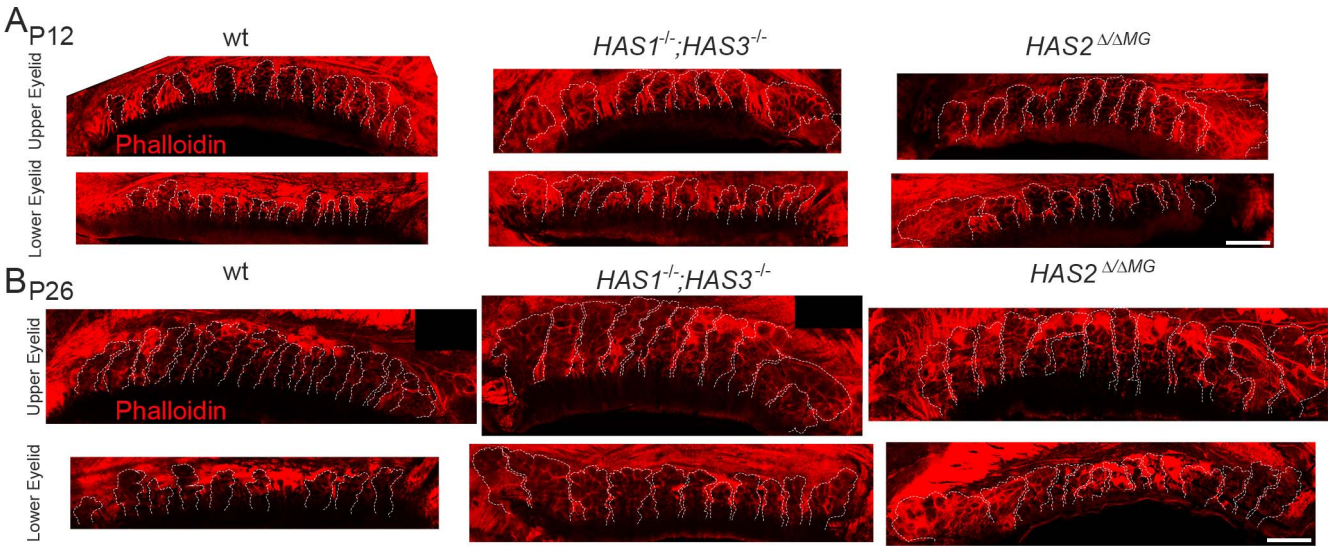

Figure 9. Whole eyelids were obtained from wt, *HAS1*$^{-/-}$;*HAS3*$^{-/-}$, and *HAS2*$^{\Delta/\Delta MG}$ mice at PD12 (**A**) and PD26 (**B**), fixed, trimmed, stained with phalloidin (*red*), and mounted to enable flat mount. The upper and lower eyelids were scanned under a confocal microscope. A *white dashed line* has been used to outline the developing MG. *Scale bar* represents 500 μm.

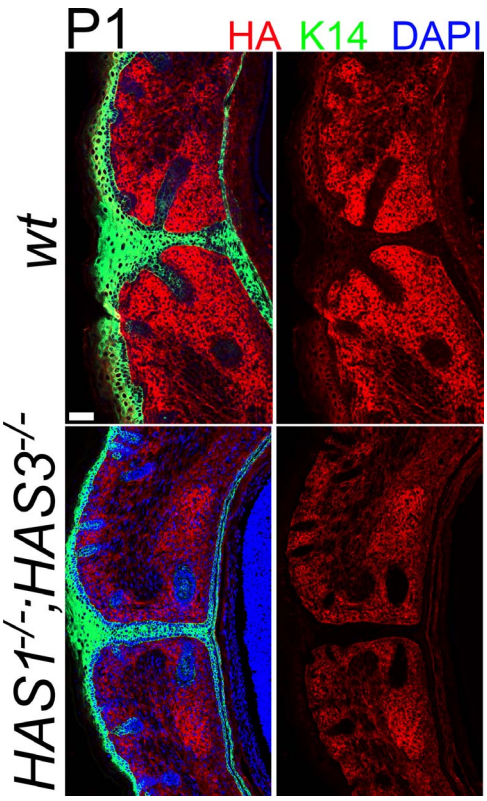

FIGURE 10. HA (*red*) and K14 (*green*) staining in sagittal sections of eyelids from wt, *HAS1*$^{-/-}$;*HAS3*$^{-/-}$, and *HAS2*$^{A/\Delta MG}$ mice at PD1. Staining revealed that HA is present throughout the mesenchymal component of the eyelid, and that HA expression is strongest at the tip of the eyelid. K14 staining reveals the developing MG growing into the HA-rich eyelid. Nuclei were counterstained with DAPI (*blue*). *Scale bar*: 50 μm.

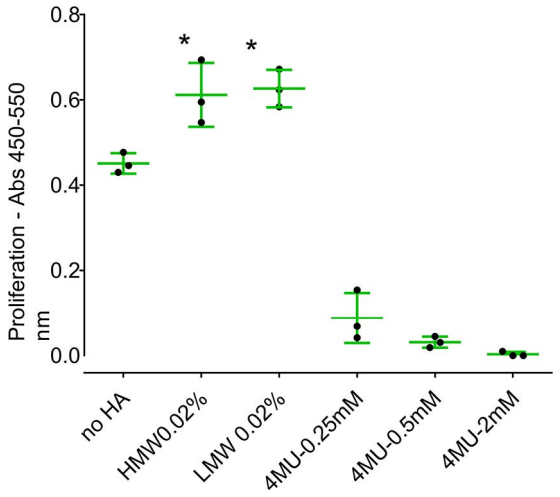

FIGURE 11. The effect of HA on the proliferation of hMGCs was assayed in vitro by measuring BrdU incorporation. The hMGCs were seeded in the presence of 0.01% HMWHA; 0.01% LMWHA; 0.25 mM, 0.5 mM, 1 mM, or 2 mM 4-MU; or PBS as a vehicle control. After 24 hours, while the cells were in their exponential growth phase, BrdU was added to each well and left for 2 hours. Both HMWHA and LMWHA significantly promoted the proliferation of hMGCs, while 4-MU significantly inhibited proliferation at all concentrations used. $^{*}P \leq 0.05$.

and reach the center of the acinus, they disintegrate and release portions of their cytoplasm containing the meibum into glandular ductules. Interestingly, the EdU^{+} cells within the MG are present within the HA-rich matrix (Fig. 12). Thus, together, our in vitro and in vivo data suggest that the HA matrix that surrounds the MGs could serve to support the highly proliferative cells. Moreover, as the meibocytes move centripetally, the loss of the HA matrix could trigger the maturation of these cells.

Differentiation Assay

To verify whether HA could play a role in regulating the differentiation of MG progenitor cells and lipid production, we used the hMGC differentiation assay. Lipid droplets accumulated in the cytoplasm of hMGCs cultured in differentiation media; however, the addition of HMWHA, LMWHA, ULMWHA, or 4-MU to the differentiation media inhibited lipid production (Figs. 13A, 13B). Seeding hMGCs on culture dishes coated with HMWHA or LMWHA also inhibited lipid production in comparison with control cells (Figs. 13C, 13D).

Hanging Drop Assay

To investigate whether HA surrounding the MGs plays a role in MG formation and differentiation, we used the hanging drop assay for the generation of a 3D culture system (Fig. 14). The hanging drop method involves culturing cells in a drop until they aggregate to form spheroids, after which they may proceed to form tissue-like cell aggregates and structures.[52] After 4 days in serum-free culture conditions, MG epithelial cells formed nondense clusters (Fig. 14A). Interestingly, when the MG epithelial cells were cultured in the presence of HMWHA, they formed tube-like tissue structures with the formation of small spheroids emerging from the tube-like structures (Figs. 14A, 14B). In the presence of LMWHA, MG epithelial cells also organized into tube-like structures, with small spheroids emerging from the tube-like structures, although the network was not as dense as that observed with HMWHA (Fig. 14A). When MG epithelial cells were cultured in the presence of ULMWHA, they formed nondense clusters similar to those observed with control untreated cells. The MG cells were then cultured for a further 6 days in the presence of FBS to trigger differentiation, culminating in a total of 10 days in vitro. When cultured in the presence of FBS, 50% of the untreated-control drops containing MG epithelial cells formed a nondense cluster of cells, while the other 50% formed a spheroid (shown in Fig. 14C). In the presence of serum and HMWHA, 100% of the drops containing MG epithelial cells formed a spheroid. In the presence of LMWHA and ULMWHA, the MG epithelial cells formed significantly smaller spheroids (Fig. 14C). After 10 days in vitro, the largest spheroid in each drop was measured, fixed, and processed for immunostaining. HMWHA induced the formation of significantly larger spheroids, when compared with the untreated control, LMWHA, and ULMWHA (Fig. 14D). In general, when using the hanging drop assay, factors that promote the formation of spheroids can be considered positive regulators of the developmental process.[53,54] Thus, HMWHA could be considered to be a positive cue for development of the MG. Interestingly, phalloidin staining revealed that in the center of the spheroids, the MG epithelial cells started to form acini (Fig. 14E). A single acinus was seen in the center of control spheres, whereas multiple acini were observed within the HMWHA treated spheres, thus further confirming that HA promotes development of the MG (Fig. 14E). The ULMWHA-treated spheres, even though

Investigative Ophthalmology & Visual Science

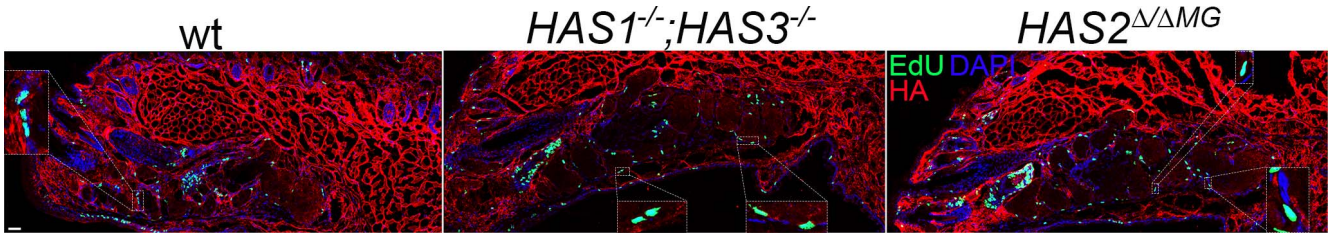

Figure 12. In order to evaluate the effect of HA on MG proliferation, wt, *HAS1*$^{-/-}$;*HAS3*$^{-/-}$, and *HAS2*$^{\Delta/\Delta MG}$ mice were treated with EdU. EdU^{+} cells were located within the HA matrix of the MG. Selected areas containing EdU^{+} cells have been outlined in the figure with a *white dashed box* and a magnified image of the selected area presented within the figure. *Scale bar*: 50 μm.

smaller than the control spheres, also presented multiple acini (Fig. 14E). Interestingly, as seen in vivo, HA^{+} meibocytes were present in the outer layers of control spheroids, circumventing the developing acinus (Fig. 14F). Thus, a subset of meibocytes differentiate into HA-expressing cells and are present in the outer layers of the spheroids (Fig. 14F).

Discussion

This study investigated the role of HA in eyelid and MG development and function. Our findings show, for the first time, that an HA-rich network surrounds the basal layer of MG acini and that the tarsal plate is an HA-rich tissue. Modifying HA

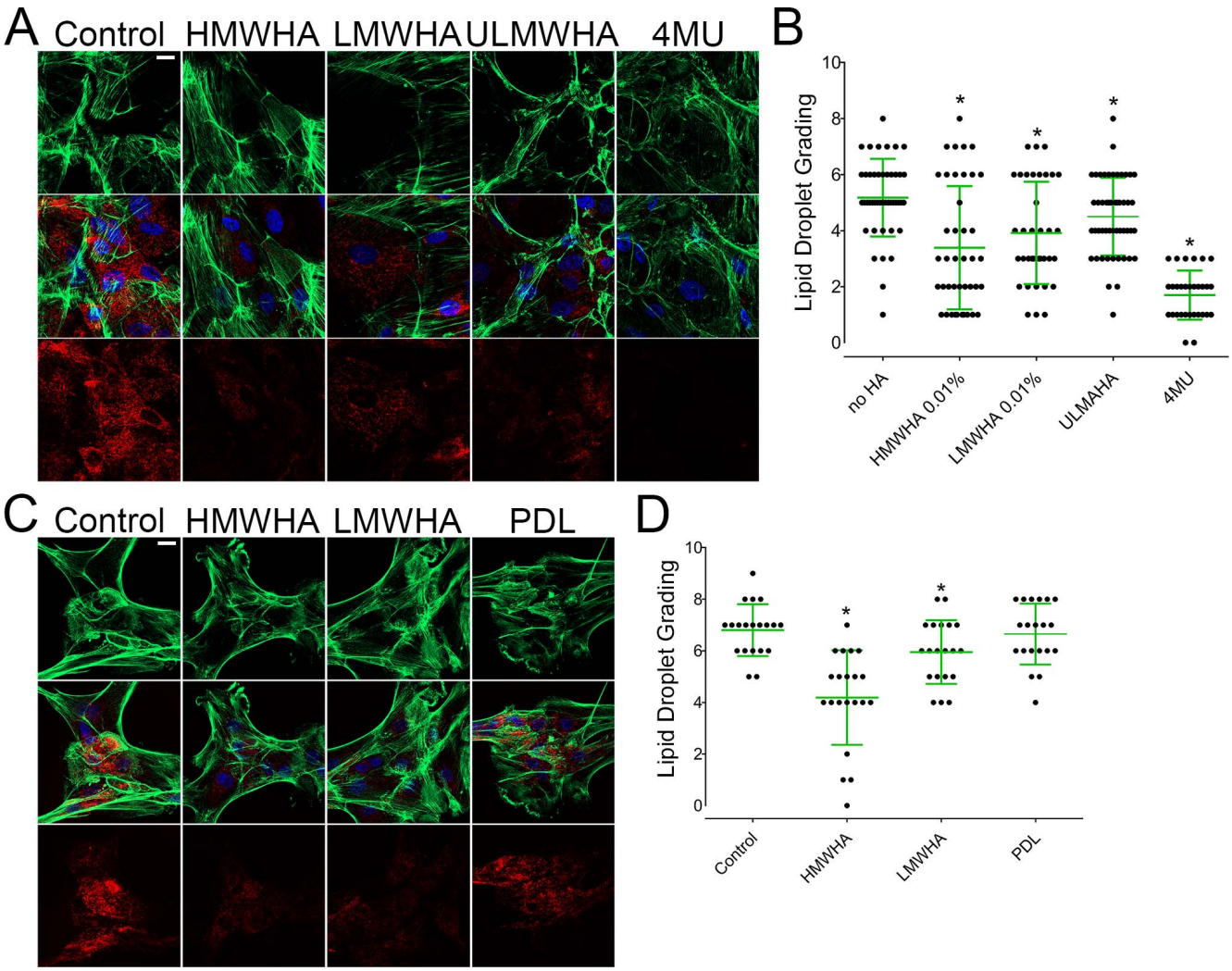

Figure 13. To evaluate the effect of HA on MG differentiation, hMGCs were maintained in culture for 2 days in differentiation media in the presence or not of 0.05% HMWHA, 0.05% LMWHA, 0.01% ULMWHA, or 0.5 mM 4-MU (**A**). Once lipid droplets were evident in the control cells, LipidTOX was added for a remaining 24 hours, after which the cells were fixed and counter stained with phalloidin and DAPI. The quantity of lipid droplets was assayed by two separate investigators in a blinded manner (**B**). Alternatively, hMGCs were seeded on cover slips previously coated with HMWHA or LMWHA (**C**), and the number of lipid droplets assayed (**D**). *Scale bar*: 20 μm. *$P \leq 0.05$.

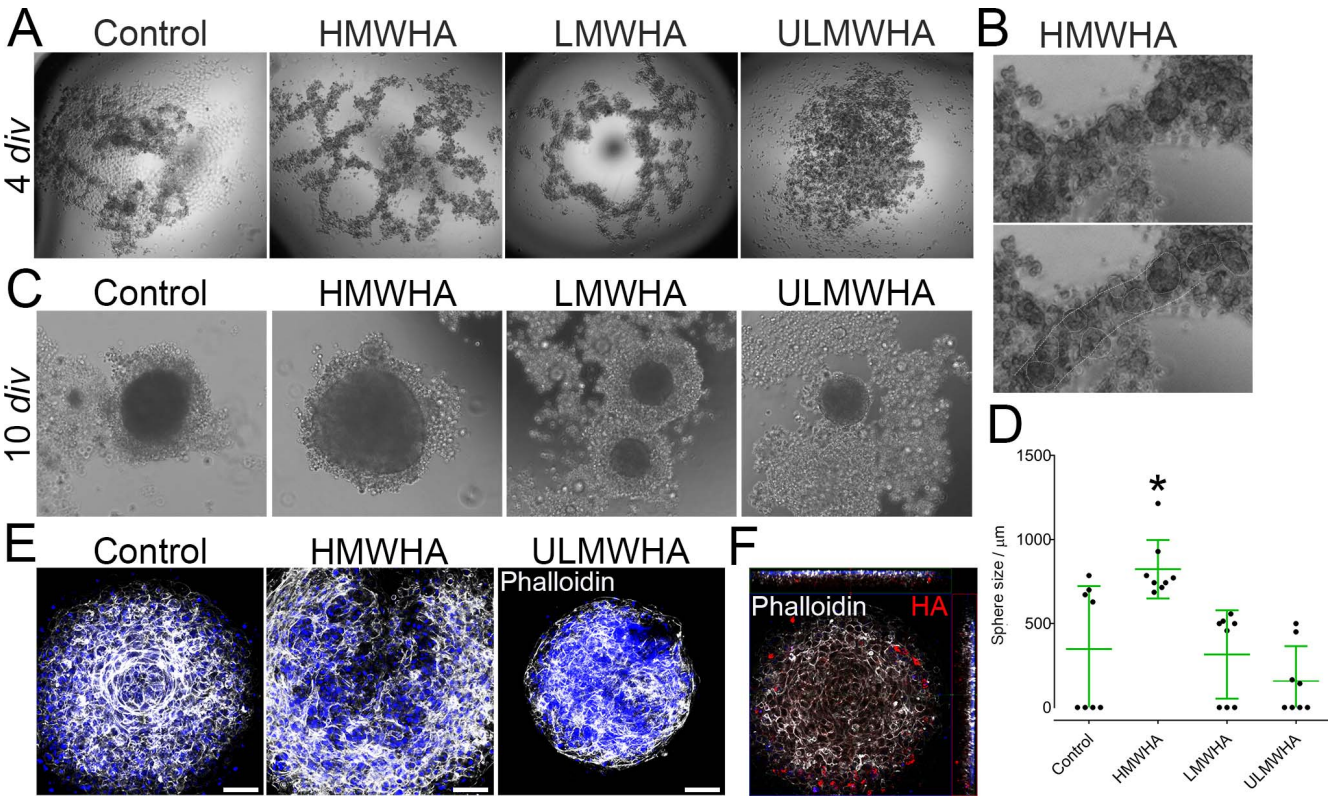

Figure 14. The 3D hanging drop culture system was used to determine the role of HA in MG development. Ten-microliter drops of hMGCs were placed on the inside of a petri dish lid in the presence or absence of 0.05% HMWHA, 0.05% LMWHA, or 0.01% ULMWHA. The cells were maintained in culture for 4 days under serum-free conditions and images were collected (**A**). Thereafter, FBS was added at a final concentration of 10% to trigger differentiation and images captured after 6 days after a total of 10 days in vitro (div) (**B**, **C**). The size of the largest sphere in each drop was measured at 10 div, and HMWHA treated spheres were significantly larger in size (**D**). The spheres were fixed after 10 div and stained with phalloidin (*white*) and HA (*red*) (**E**, **F**). In control spheres, the development of an acinus could be noted in the center of the sphere, whereas in HMWHA- and ULMWHA-treated spheres, the formation of multiple acini was seen within the sphere (**E**). Cells in the outer layers of the spheres differentiated into HA-producing cells (**F**). Nuclei were counterstained with DAPI (*blue*). *Scale bar*: 50 µm. $^*P \leq 0.05$.

levels within the eyelid leads to an increase in size and morphologic alterations of the MG, demonstrating that HA regulates MG morphogenesis.

HA is a ubiquitous component of cells and tissues and has been extensively shown to play a vital role in development, inflammation, and pathology.[20,21,23–26] HA is a polysaccharide that interacts with a wide variety of bioactive ligands, such as growth factors, morphogens and their receptors, ECM proteins, proteases, cytokines, chemokines, and enzyme inhibitors.[18,19,25,55] The specificity of the interactions between HA and the plethora of ligands is dictated largely by the length of the HA chain. The two most widely distributed forms of HA are HMWHA and LMWHA, both of which are synthesized by HASs.[33,56,57] The biosynthesis of HA differs from that of other members of the glycosaminoglycan family, which are synthesized upon a protein core in the Golgi complex. In contrast, HA biosynthesis takes place in the cytoplasm. The HAS enzymes are located at the plasma membrane and the growing HA is gradually released into the ECM during chain elongation. Basic understanding of how the HAS enzymes regulate the length of the growing HA chain during the biosynthetic process, which drastically affects its physiologic function, remains unknown. As the HA chain is synthesized, it is incorporated into the ECM, and some groups have hypothesized that the stiffness of the tissue during pathogenesis could lead to a greater "pulling force" on the growing HA chain, which would lead to the production of shorter HA chains.[58] It has also been speculated that HAS1 and HAS2 produce primarily HMWHA, whereas HAS3 produces primarily LMWHA; however, some groups have shown that all HAS isoforms have the ability make both HMWHA and LMWHA.[35] Interestingly, the *Has* knockout mice used in this study did not display a loss of HA in the eyelids. Therefore, the *HAS1*$^{-/-}$;*HAS3*$^{-/-}$ mice upregulate *Has*2 through a compensatory mechanism, whereas the *HAS2*$^{\Delta/\Delta MG}$ mice upregulate *Has1* and/or *3* thereby preventing a loss of HA. We speculate that changes in the *Has* expression profile in the knockout mice could lead to changes in HMWHA versus LMWHA distribution in the eyelid, and, therefore, the observed phenotype would be a result of changes in the form of HA present and not due to a loss of HA. Moreover, changes in HAS expression could also alter the ultrastructure of the HA network surrounding the MG basal cells. Further studies will work toward deciphering the code behind HA chain length regulation during eyelid and MG development.

To date, limited studies have been dedicated to studying the MG and eyelid ECM. To the best of our knowledge the only previous study investigated the ECM composition within the tarsal plate by using immunohistochemistry.[59] The authors carried out a histologic analysis of human eyelids with a number of antibodies against ECM components.[59] They demonstrated that collagen types I, III, and VI; aggrecan; versican; and tenascin were strongly expressed in the tarsal plate.[59] These authors also showed that there was strong labeling for aggrecan, dermatan sulfate, and chondroitin 6-sulfate immediately surrounding the MGs.[59] Aggrecan, versi-

can, and tenascin are all hyaladherins and are generally found in tissues bound to HA-forming macromolecules that stabilize various matrices, such as in the bone and cartilage.[60,61] These authors did not, however, investigate the staining pattern of HA in their study. Our work shows for the first time that HA is strongly expressed in the tarsal plate and that an HA matrix surrounds the basal cell layer of the MGs. We also show that HA is highly expressed within the mesenchymal component of the eyelid during eyelid development. *HAS1*$^{-/-}$;*HAS3*$^{-/-}$ and *HAS2*$^{\Delta/\Delta MG}$ mice display precocious Meibomian budding during development and the adult mice present enlarged and elongated MG with an increased volume, primarily due to an increase in the number and size of acini. Excessive budding was noted in *HAS1*$^{-/-}$;*HAS3*$^{-/-}$ and *HAS2*$^{\Delta/\Delta MG}$ mice by PD26, to the extent that there was no longer conjunctival tissue between individual MGs. Thus, our data suggest that an HA-rich mesenchyme plays a role during MG development and remodeling as a key regulator in the acinar budding process. Exacerbated acinar budding in *HAS1*$^{-/-}$;*HAS3*$^{-/-}$ and *HAS2*$^{\Delta/\Delta MG}$ mice leads to the formation of enlarged and dysmorphic glands. Our data also demonstrate that HA plays a vital role in MG homeostasis, supporting proliferative MG precursor cells.

MGs are holocrine glands, meaning that meibocytes synthesize and accumulate lipids until they eventually undergo degeneration and disintegration as they discharge the meibum. Thus, the MGs must constantly replenish acinar cells that are destroyed as part of the secretory process. This requires that MG precursor cells in the basal layer proliferate and move centripetally, thereby providing a constant supply of newly maturing MG cells. Our findings show that the highly proliferative MG precursor cells are located within an HA-rich ECM. Together, our in vitro and in vivo data suggest that the HA matrix supports the MG precursor cells in the proliferative state. The hanging drop assay has been developed as a 3D in vitro cell culture model that more closely mimics in vivo conditions. In this culture system, the cells form a spheroid containing a closely packed cell mass enabling cells to establish an intimate, direct cell-cell adhesion architecture with neighboring cells and with ECM components. Interestingly, MG cells developed an acinus within the center of the spheroid, and in the outer layers of the spheroid, a subset of MG cells differentiated into HA-producing cells, which over time encapsulated the acini with an HA-rich matrix. Thus, our findings suggest that the encapsulation of MG acini with HA plays an important role in the developmental process. Interestingly, when the spheroids were treated with HMWHA, numerous acini were formed within each spheroid, as opposed to a single acinus as seen in the control spheroids, suggesting that HA triggers the formation of MG acini during development.

The continual turnover of acinar cells throughout life would eventually extinguish the proliferative precursor MG cells at the basal layer of the MG.[62] Thus, it has been hypothesized that the basal layer of the MG would require constant renewal with younger cells. The MG stem cell niche is poorly described, unlike the hair follicle, containing the bulge that maintains slow-cycling progenitors.[6,7] Limited studies have described putative stem cell populations within the MG.[62–64] However, it has recently been shown by using H2B-GFP/K5tTA mice that slow-cycling progenitor cells are present within the MG terminal ducts that transition into acinus (ductule).[5] Here, we also used H2B-GFP/K5tTA mice to confirm that acinar progenitor cells or slow-cycling MG stem cell-like cells are located within the HA-rich niches. We hypothesize that, as seen in other stem cell niches, the HA scaffold could help to keep the progenitor cells in an undifferentiated state of reversible cell cycle arrest.

The eyelid is a specialized form of skin, which is much thinner than regular skin. The eyelid contains all skin structures on the anterior surface of the eyelid, with the exception of subcutaneous fat. Eyelids contain a tarsal plate, which is a firm plate composed of dense connective tissue in which the MGs are embedded. The palpebral conjunctiva is located on the posterior eyelid surface and is lined by epithelial cells followed by a subepithelial stroma, the substantia propria. The epithelium of the tarsal conjunctiva is mostly cuboidal and contains goblet cells. The eyelid plays a vital role in ocular surface development and homeostasis. Eyelids are crucial for the development of MGs, lacrimal glands, conjunctival tissue, and extraocular muscles, and eye-open-at birth studies have demonstrated the importance of eyelids for both corneal and lens development.[65] Eyelids also play an important role in maintaining ocular surface homeostasis, for example serving as the first line of defense for the ocular surface as a physical barrier against foreign objects, spreading the tear film over the ocular surface, and also preventing tear evaporation, which is particularly important during sleep. Eyelid damage or abnormalities may lead to numerous ocular diseases, such as MGD, blepharitis, blepharophimosis, eyelid coloboma, congenital eyelid imbrication syndrome, and lagophthalmos. MGD can be caused by a blockage of glands, alteration of glands, or loss of glands, all which culminate in a decrease or alteration in the lipid content of the tear film. Tear film instability leads to evaporation of the aqueous layer, increasing tear osmolality. MGD is the leading cause of dry eye disease, which affects approximately 60% of the population. Blepharitis is an eyelid disorder characterized by congested MGs that leads to itchiness, ocular irritation, and tear film instability, and accounts for 47% of ophthalmic complaints in the clinical setting. Blepharitis is a common secondary disorder to MGD, thus many MGD patients eventually develop blepharitis. Although a strong correlation exists between MGD and blepharitis, the relationship between the two conditions remains to be established. MGD patients are commonly treated with HA in the form of eye drops, which has been shown to be effective for alleviating the symptoms. However, whether a correlation exists between HA-treated MGD patients and blepharitis remains to be elucidated. Epithelial hyperplasia is the most common benign eyelid lesion and results in hyperplastic growths arising from the epidermis. The *HAS1*$^{-/-}$;*HAS3*$^{-/-}$ and *HAS2*$^{\Delta/\Delta MG}$ mice developed epithelial hyperplasia along the palpebral conjunctiva. Interestingly, all mice analyzed presented some extent of palpebral conjunctival epithelial hyperplasia, developing prominent papules or nodules. The epithelial hyperplasia presented by *HAS1*$^{-/-}$;*HAS3*$^{-/-}$ and *HAS2*$^{\Delta/\Delta MG}$ mice were not initially noted macroscopically but were identified microscopically by histology. Thus, whether patients that are treated with eye drops containing HA as an active component develop epithelial hyperplasia should be explored in a clinical setting.

Over the past decade, there has been an increased pharmaceutical interest in HA, and many cosmetic products and Food and Drug Administration-approved medications, such as eye drops, currently contain HA as an active component. In recent years, the use of HA in ophthalmic products has grown exponentially, and of particular interest is the growing trend to add HA to eye drops for treating dry eye. Therefore, it is of vital importance to characterize both the expression profile and function of HA on the ocular surface before we can fully appreciate the potential impact of the long-term use of HA-based eye drops. This work is the first to show that HA is constitutively expressed in the basal layer of the MG and supports proliferating MG precursor cells. Moreover, changes in HA levels within the tarsal plate lead to the formation of dysmorphic enlarged MGs. Importantly, changes in HA levels

Investigative Ophthalmology & Visual Science

lead to epidermal hyperplasia and the formation of epidermal outgrowths along the palpebral conjunctiva. Thus, our work suggests that clinicians should monitor patients using HA-based eye drops for epidermal hyperplasia and outgrowths in the palpebral conjunctival region that could lead to the loss of a smooth wiping surface. Moreover, our work lays the foundation for other studies to establish the role the eyelid ECM may play in ocular disorders for which the underlying pathogenesis remains elusive, such as the floppy eyelid syndrome.

Acknowledgments

The authors thank Vincent Hascall, Yvette M. Coulson-Thomas, Tarsis Ferreira, and James Jester for their valuable support throughout the study. The authors also thank Naoki Itano for providing HAS1 null mice, Winston Kao for providing the K14 rtta and tet-Ocre mice, Adam Glick for providing the K5tTA mice, and David Sullivan for the hMGCs.

Supported by start-up funds from the University of Houston, the Mizutani Foundation, and the National Institutes of Health/ National Eye Institute Core Grant P30 EY07551.

Disclosure: **M. Sun**, None; **S. Puri**, None; **G.J. Parfitt**, None; **N. Mutoji**, None; **V.J. Coulson-Thomas**, None

References

1. Jester JV, Nicolaides N, Smith RE. Meibomian gland studies: histologic and ultrastructural investigations. *Invest Ophthalmol Vis Sci*. 1981;20:537–547.
2. Tektas OY, Yadav A, Garreis F, et al. Characterization of the mucocutaneous junction of the human eyelid margin and meibomian glands with different biomarkers. *Ann Anat*. 2012;194:436–445.
3. Paulsen F, Garreis F. What drives Meibomian gland disease? [in Spanish]. *Arch Soc Esp Oftalmol*. 2014;89:175–176.
4. Gorgas K, Volkl A. Peroxisomes in sebaceous glands. IV. Aggregates of tubular peroxisomes in the mouse Meibomian gland. *Histochem J*. 1984;16:1079–1098.
5. Parfitt GJ, Lewis PN, Young RD, et al. Renewal of the holocrine meibomian glands by label-retaining, unipotent epithelial progenitors. *Stem Cell Rep*. 2016;7:399–410.
6. Cotsarelis G, Sun TT, Lavker RM. Label-retaining cells reside in the bulge area of pilosebaceous unit: implications for follicular stem cells, hair cycle, and skin carcinogenesis. *Cell*. 1990;61:1329–1337.
7. Tumbar T, Guasch G, Greco V, et al. Defining the epithelial stem cell niche in skin. *Science*. 2004;303:359–363.
8. Smith TG, Sweetman D, Patterson M, Keyse SM, Munsterberg A. Feedback interactions between MKP3 and ERK MAP kinase control scleraxis expression and the specification of rib progenitors in the developing chick somite. *Development*. 2005;132:1305–1314.
9. You S, Tariq A, Kublin CL, Zoukhri D. Detection of BrdU-label retaining cells in the lacrimal gland: implications for tissue repair. *Cell Tissue Res*. 2011;346:317–326.
10. Zhang H, Boddupally K, Kandyba E, et al. Defining the localization and molecular characteristic of minor salivary gland label-retaining cells. *Stem Cells*. 2014;32:2267–2277.
11. Nichols KK, Foulks GN, Bron AJ, et al. The international workshop on meibomian gland dysfunction: executive summary. *Invest Ophthalmol Vis Sci*. 2011;52:1922–1929.
12. Schaumberg DA, Nichols JJ, Papas EB, Tong L, Uchino M, Nichols KK. The international workshop on meibomian gland dysfunction: report of the subcommittee on the epidemiology of, and associated risk factors for, MGD. *Invest Ophthalmol Vis Sci*. 2011;52:1994–2005.
13. Den S, Shimizu K, Ikeda T, Tsubota K, Shimmura S, Shimazaki J. Association between meibomian gland changes and aging, sex, or tear function. *Cornea*. 2006;25:651–655.
14. Jie Y, Xu L, Wu YY, Jonas JB. Prevalence of dry eye among adult Chinese in the Beijing Eye Study. *Eye*. 2009;23:688–693.
15. Korb DR, Henriquez AS. Meibomian gland dysfunction and contact lens intolerance. *J Am Optom Assoc*. 1980;51:243–251.
16. Caglar C, Senel E, Sabancilar E, Durmus M. Reduced ocular surface disease index (OSDI) scores in patients with isotretinoin treatment. *Int Ophthalmol*. 2017;37:197–202.
17. Liang L, Liu Y, Ding X, Ke H, Chen C, Tseng SCG. Significant correlation between meibomian gland dysfunction and keratitis in young patients with Demodex brevis infestation [published online ahead of print October 21, 2017]. *Br J Ophthalmol*. doi:10.1136/bjophthalmol-2017-310302.
18. Rogers HJ. An analysis of the products formed during the hydrolysis of hyaluronate by enzymes and acids, with observations on the nature of the amino-sugar released from the polysaccharide. *Biochem J*. 1946;40:782–788.
19. Lamberg SI, Yuspa SH, Hascall VC. Synthesis of hyaluronic acid is decreased and synthesis of proteoglycans is increased when cultured mouse epidermal cells differentiate. *J Invest Dermatol*. 1986;86:659–667.
20. Cantor JO, Cerreta JM, Armand G, Osman M, Turino GM. The pulmonary matrix, glycosaminoglycans and pulmonary emphysema. *Connect Tissue Res*. 1999;40:97–104.
21. Culley FJ, Fadlon EJ, Kirchem A, Williams TJ, Jose PJ, Pease JE. Proteoglycans are potent modulators of the biological responses of eosinophils to chemokines. *Eur J Immunol*. 2003;33:1302–1310.
22. Jiang D, Liang J, Noble PW. Hyaluronan in tissue injury and repair. *Ann Rev Cell Dev Biol*. 2007;23:435–461.
23. Negrini D, Passi A, Moriondo A. The role of proteoglycans in pulmonary edema development. *Intensive Care Med*. 2008; 34:610–618.
24. Jiang D, Liang J, Noble PW. Regulation of non-infectious lung injury, inflammation, and repair by the extracellular matrix glycosaminoglycan hyaluronan. *Anat Rec*. 2010;293:982–985.
25. Misra S, Hascall VC, Markwald RR, Ghatak S. Interactions between hyaluronan and its receptors (CD44, RHAMM) regulate the activities of inflammation and cancer. *Front Immunol*. 2015;6:201.
26. Nicholls MA, Fierlinger A, Niazi F, Bhandari M. The disease-modifying effects of hyaluronan in the isteoarthritic disease state. *Clinical Med Insights Artbritis Musculoskelet Disord*. 2017;10:1179544117723611.
27. Coulson-Thomas VJ, Gesteira TF, Hascall V, Kao W. Umbilical cord mesenchymal stem cells suppress host rejection: the role of the glycocalyx. *Journal Biol Chem*. 2014;289:23465–23481.
28. Coulson-Thomas YM, Gesteira TF, Norton AL, Kao WW, Nader HB, Coulson-Thomas VJ. The role of proteoglycans in the reactive stroma on tumor growth and progression. *Histol Histopathol*. 2015;30:33–41.
29. Gesteira TF, Sun M, Coulson-Thomas YM, et al. Hyaluronan rich microenvironment in the limbal stem cell niche regulates limbal stem cell differentiation. *Invest Ophthalmol Vis Sci*. 2017;58:4407–4421.
30. Wight TN, Frevert CW, Debley JS, Reeves SR, Parks WC, Ziegler SF. Interplay of extracellular matrix and leukocytes in lung inflammation. *Cell Immunol*. 2017;312:1–14.
31. Chowdhury B, Xiang B, Liu M, Hemming R, Dolinsky VW, Triggs-Raine B. Hyaluronidase 2 deficiency causes increased mesenchymal dells, congenital heart defects, and heart failure. *Circ Cardiovasc Genet*. 2017;10:e001598.

32. McDonald J, Hascall VC. Hyaluronan minireview series. *J Biol Chem*. 2002;277:4575–4579.
33. Lee JY, Spicer AP. Hyaluronan: a multifunctional, megaDalton, stealth molecule. *Curr Opin Cell Biol*. 2000;12:581–586.
34. Bart G, Vico NO, Hassinen A, et al. Fluorescence resonance energy transfer (FRET) and proximity ligation assays reveal functionally relevant homo- and heteromeric complexes among hyaluronan synthases HAS1, HAS2, and HAS3. *J Biol Chem*. 2015;290:11479–11490.
35. Weigel PH, Baggenstoss BA. Hyaluronan synthase polymerizing activity and control of product size are discrete enzyme functions that can be uncoupled by mutagenesis of conserved cysteines. *Glycobiology*. 2012;22:1302–1310.
36. Baggenstoss BA, Harris EN, Washburn JL, Medina AP, Nguyen L, Weigel PH. Hyaluronan synthase control of synthesis rate and hyaluronan product size are independent functions differentially affected by mutations in a conserved tandem B-X7-B motif. *Glycobiology*. 2017;27:154–164.
37. Tian X, Azpurua J, Hine C, et al. High-molecular-mass hyaluronan mediates the cancer resistance of the naked mole rat. *Nature*. 2013;499:346–349.
38. Knop N, Knop E. Meibomian glands. Part I: anatomy, embryology and histology of the Meibomian glands [in German]. *Ophthalmologe*. 2009;106:872–883.
39. Nien CJ, Massei S, Lin G, et al. The development of meibomian glands in mice. *Mol Vis*. 2010;16:1132–1140.
40. Underhill CB. Hyaluronan is inversely correlated with the expression of CD44 in the dermal condensation of the embryonic hair follicle. *J Invest Dermatol*. 1993;101:820–826.
41. Agren UM, Tammi M, Ryynanen M, Tammi R. Developmentally programmed expression of hyaluronan in human skin and its appendages. *J Invest Dermatol*. 1997;109:219–224.
42. Wang C, Tammi M, Tammi R. Distribution of hyaluronan and its CD44 receptor in the epithelia of human skin appendages. *Histochemistry*. 1992;98:105–112.
43. Kalabusheva E, Terskikh V, Vorotelyak E. Hair germ model in vitro via human postnatal keratinocyte-dermal papilla interactions: impact of hyaluronic acid. *Stem Cells Int*. 2017;2017:9271869.
44. Matsumoto K, Li Y, Jakuba C, et al. Conditional inactivation of Has2 reveals a crucial role for hyaluronan in skeletal growth, patterning, chondrocyte maturation and joint formation in the developing limb. *Development*. 2009;136:2825–2835.
45. Fulop C, Szanto S, Mukhopadhyay D, et al. Impaired cumulus mucification and female sterility in tumor necrosis factor-induced protein-6 deficient mice. *Development*. 2003;130:2253–2261.
46. Perl AK, Wert SE, Nagy A, Lobe CG, Whitsett JA. Early restriction of peripheral and proximal cell lineages during formation of the lung. *Proc Natl Acad Sci U S A*. 2002;99:10482–10487.
47. Spicer AP, McDonald JA. Characterization and molecular evolution of a vertebrate hyaluronan synthase gene family. *J Biol Chem*. 1998;273:1923–1932.
48. Gesteira TF, Coulson-Thomas YM, Coulson-Thomas VJ. Anti-inflammatory properties of the glial scar. *Neural Regen Res*. 2016;11:1742–1743.
49. Diamond I, Owolabi T, Marco M, Lam C, Glick A. Conditional gene expression in the epidermis of transgenic mice using the tetracycline-regulated transactivators tTA and rTA linked to the keratin 5 promoter. *J Invest Dermatol*. 2000;115:788–794.
50. Sullivan DA, Liu Y, Kam WR, et al. Serum-induced differentiation of human meibomian gland epithelial cells. *Invest Ophthalmol Vis Sci*. 2014;55:3866–3877.
51. Coulson-Thomas VJ, Coulson-Thomas YM, Gesteira TF, Kao WW. Extrinsic and intrinsic mechanisms by which mesenchymal stem cells suppress the immune system. *Ocul Surf*. 2016;14:121–134.
52. Foty R. A simple hanging drop cell culture protocol for generation of 3D spheroids. *J Vis Exp*. 2011;51:2720.
53. Bartosh TJ, Ylostalo JH, Mohammadipoor A, et al. Aggregation of human mesenchymal stromal cells (MSCs) into 3D spheroids enhances their antiinflammatory properties. *Proc Natl Acad Sci U S A*. 2010;107:13724–13729.
54. Klaka P, Grudl S, Banowski B, et al. A novel organotypic 3D sweat gland model with physiological functionality. *PLoS One* 2017;12:e0182752.
55. Toole BP. Hyaluronan and its binding proteins, the hyaladherins. *Curr Opin Cell Biol*. 1990;2:839–844.
56. Stern R, Asari AA, Sugahara KN. Hyaluronan fragments: an information-rich system. *Eur J Cell Biol*. 2006;85:699–715.
57. Torronen K, Nikunen K, Karna R, Tammi M, Tammi R, Rilla K. Tissue distribution and subcellular localization of hyaluronan synthase isoenzymes. *Histochem Cell Biol*. 2014;141:17–31.
58. Cowman MK. Hyaluronan and hyaluronan fragments. *Adv Carbohydr Chem Biochem*. 2017;74:1–59.
59. Milz S, Neufang J, Higashiyama I, Putz R, Benjamin M. An immunohistochemical study of the extracellular matrix of the tarsal plate in the upper eyelid in human beings. *J Anat*. 2005;206:37–45.
60. Olin AI, Morgelin M, Sasaki T, Timpl R, Heinegard D, Aspberg A. The proteoglycans aggrecan and Versican form networks with fibulin-2 through their lectin domain binding. *J Biol Chem*. 2001;276:1253–1261.
61. Galtrey CM, Kwok JC, Carulli D, Rhodes KE, Fawcett JW. Distribution and synthesis of extracellular matrix proteoglycans, hyaluronan, link proteins and tenascin-R in the rat spinal cord. *Eur J Neurosci*. 2008;27:1373–1390.
62. Olami Y, Zajicek G, Cogan M, Gnessin H, Pe'er J. Turnover and migration of meibomian gland cells in rats' eyelids. *Ophthalmic Res*. 2001;33:170–175.
63. Knop E, Knop N, Millar T, Obata H, Sullivan DA. The international workshop on meibomian gland dysfunction: report of the subcommittee on anatomy, physiology, and pathophysiology of the meibomian gland. *Invest Ophthalmol Vis Sci*. 2011;52:1938–1978.
64. Parfitt J, Harris M, Wright JM, Kalamchi S. Tumor suppressor gene mutation in a patient with a history of hyperparathyroidism-jaw tumor syndrome and healed generalized osteitis fibrosa cystica: a case report and genetic pathophysiology review. *J Oral Maxillofac Surg*. 2015;73:194.e1–e9.
65. Carmona FD, Ou J, Jimenez R, Collinson JM. Development of the cornea of true moles (Talpidae): morphogenesis and expression of PAX6 and cytokeratins. *J Anat*. 2010;217:488–500.

Investigative Ophthalmology & Visual Science